J Biomol NMR (2011) 51:163–171
DOI 10.1007/s10858-011-9550-0

ARTICLE

NMR detection and characterization of sialylated glycoproteins and cell surface polysaccharides

Adam W. Barb · Darón I. Freedberg · Marcos D. Battistel · James H. Prestegard

Received: 11 May 2011 / Accepted: 25 June 2011

Abstract Few solution NMR pulse sequences exist that are explicitly designed to characterize carbohydrates (glycans). This is despite the essential role carbohydrate motifs play in cell–cell communication, microbial pathogenesis, autoimmune disease progression and cancer metastasis, and despite that fact that glycans, often shed to extra-cellular fluids, can be diagnostic of disease. Here we present a suite of two dimensional coherence experiments to measure three different correlations (H3–C2, H3–C1, and C1–C2) on sialic acids, a group of nine-carbon carbohydrates found on eukaryotic cell surfaces that often play a key role in disease processes. The chemical shifts of the H3, C2, and C1 nuclei of sialic acids are sensitive to carbohydrate linkage, linkage conformation, and ionization state of the C1 carboxylate. The experiments reported include rigorous filter elements to enable detection and characterization of isotopically labeled sialic acids with high sensitivity in living cells and crude isolates with minimal interference from unwanted signals arising from the $\sim$1% ^{13}C-natural abundance of cellular metabolites. Application is illustrated with detection of sialic acids on living cells, in unpurified mixtures, and at the terminus of the *N*-glycan on the 55 kDa immunoglobulin G Fc.

A. W. Barb · J. H. Prestegard (✉)
Complex Carbohydrate Research Center, University of Georgia, 315 Riverbend Road, Athens, GA 30602, USA
e-mail: jpresteg@ccrc.uga.edu

D. I. Freedberg · M. D. Battistel
Laboratory of Bacterial Polysaccharides, Center for Biologics Evaluation and Research, Food and Drug Administration, Building 29, Room 115, 1401 Rockville Pike, HFM-428, Rockville, MD 20852, USA

Keywords *N*-acetylneuraminic acid · Sialic acid · Carbohydrate · Pulse sequence · In vivo NMR · Isotopic labeling

Introduction

Eukaryotic cell surfaces are coated with a layer of lipid-anchored and protein-linked complex carbohydrate chains (glycans) that shield the membrane and mediate signaling in response to external stimuli. They also provide ready markers for proper organismal development and the onset of disease. Glycans on stem cells were among the first markers of stem cell differentiation (Muramatsu and Muramatsu 2004), proteoglycans and mucin glycopeptides shed to the blood stream provide markers for certain types of cancer (Brockhausen 2006; Reis et al. 2010; Theocharis et al. 2010), and shed fragments of glycosaminoglycans provide indicators of osteoarthritis (Melrose et al. 2008; Witsch-Prehm et al. 1992). These carbohydrate structures are clearly essential to life and the maintenance of a quality in life, but complete characterization of glycan three dimensional structures is challenging. Relative to tools for the structural and dynamical characterization of proteins and nucleic acids, development of tools to study carbohydrates has been slow. There are two primary reasons for this. The extensive dynamic sampling of conformations by most carbohydrate chains prevents straightforward application of most structural biology techniques, and the conformational and compositional heterogeneity of glycan structures in most natural isolates inhibits crystallization and introduces a high level of complexity to spectroscopic approaches. In principle, solution NMR spectroscopy can provide a wealth of information on dynamic systems, and when combined with proper isotope labeling strategies can

reduce compositional complexities even in natural isolates. One limitation that exists, however, is the absence of specific spectroscopic experiments to take advantage of unique spectroscopic properties and isotopic labeling patterns of glycans. Here we present three new solution NMR pulse sequences to measure chemical shifts of one important glycan constituent (a sialic acid residue) that are extendable to the measurement of structural and dynamic parameters.

Sialic acids are carbohydrate residues that share a common nine-carbon motif, neuraminic acid (Varki 2009). The only sialic acid believed to be produced by humans is *N*-acetylneuraminic acid, a 9-carbon sugar that forms a pyranose ring as shown in Fig. 1. This residue is found at the (non-reducing) termini of glycans distal to the cell surface and is essential to proper growth, development and immune function (Nacher et al. 2010; Nasirikenari et al. 2006). For example, self/nonself discrimination in complex organisms occurs at the cell surface where sialic acid residues are specifically recognized by the immune system as self epitopes (Varki 2007). Notably, the influenza virus uses sialic acid in the initial attachment and invasion of host cells (Skehel and Wiley 2000). Bacteria display *N*-acetylneuraminic acids or residues with remarkable structural similarities on their outermost surface (Varki 2009), perhaps to evade the host immune system. A few of these sugars, produced by *Campylobacter jejuni* and *Escherichia coli*, are shown in Fig. 1.

Sialic acid has several properties that are well suited for studies using solution NMR spectroscopy. First, ^{13}C labels may be incorporated either in vitro using $^{13}C_U$ pyruvate to synthesize $^{13}C_{1,2,3}$-*N*-acetylneuraminic acid (Aubin and Prestegard 1993; Simon et al. 1988), or in vivo using ^{13}C glucose, ^{15}N ammonium chloride, and an *E. coli* cell line to produce ($^{13}C_U$, ^{15}N)-*N*-acetylneuraminic acid (Azurmendi et al. 2007). Isotope-enriched material may then be used to modify purified glycoproteins or added to metabolically active cells. Second, the resonance frequencies of the three carbons on the reducing end of the sugar (those introduced by the in vitro procedure) are widely dispersed and, with appropriate instrumentation, may each be manipulated discretely. The $^{13}C1$ carboxylate is found between 175 and 180 ppm, the $^{13}C2$ anomeric carbon is between 95 and 105 ppm, and the $^{13}C3$ methylene carbon is between 40 and 45 ppm (Bhattacharjee et al. 1975). Utilizing sequential coherence transfers between ^{13}C nuclei in a band-selective manner promises to provide substantial background suppression capabilities in complex samples, a feature required when observing sialic acid in the presence of living cells. Third, the C1 and C2 positions are not directly bonded to a proton and thus potentially have long spin lifetimes that will allow multiple magnetization transfer periods.

In addition to being widely dispersed and useful spectroscopic probes, the chemical shifts of the H3, C1, C2 and C3 nuclei also reflect alterations in the chemical (compositional) and conformational structure. The H3eq and C2 nuclei are sensitive to the linkage of *N*-acetylneuraminic acid, and resonances display different chemical shifts whether α2-3, α2-6 of α2-8 linked. The C2 frequency is likely also sensitive to rotation around the glycosidic bond, and the C1 carboxylate, and to a lesser extent C2 and C3, is sensitive to pH through environmentally sensitive pKas for this group (Gerken and Dearborn 1984).

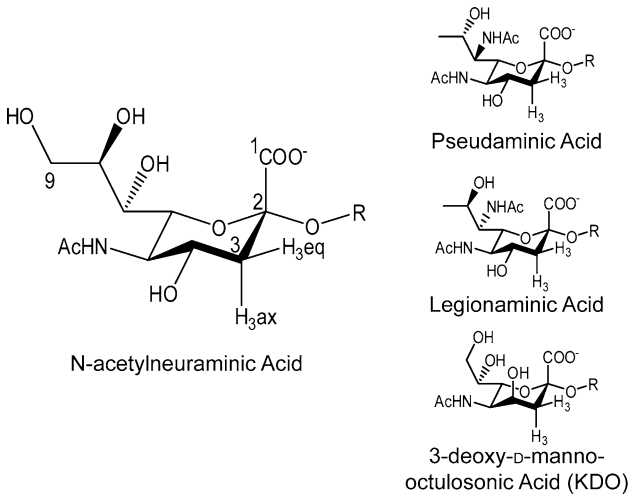

Fig. 1 Chemical structures of *N*-acetylneuraminic acid and similar carbohydrates show the unique features of these residues, including the H3 methylene protons, the non-protonated anomeric C2 and the carboxylate C1. *N*-acetylneuraminic acid is often found on eukaryotic cell surfaces at the termini of carbohydrate chains. Pathogens display this carbohydrate as well as residues with a high degree of structural similarity, including the three sugars shown on the *right*, potentially to evade host defense systems

We developed three pulse sequences to characterize sialic acid resonances with high specificity in purified samples, unpurified cell lysates and living cells. These sequences include multiple elements to filter unwanted signals arising from natural ^{13}C abundance in cellular metabolites, a requirement for observation of small soluble sialic acid carrying metabolites in unpurified samples. *N*-acetylneuraminic acid is also found on a wide variety of larger molecular assemblies including glycolipids in membrane fragments, glycoproteins and capsular polysaccharide. The sequences presented are applicable to a wide range of these larger sialylated glycoconjugate studies, as illustrated by work on the glycosylated Fc domain of immunoglobulin IgG.

Materials and methods

Preparation of ^{13}C-labeled *E. coli* cultures

All materials, unless otherwise noted, were obtained from Sigma (St. Louis, MO). A single colony of *E. coli* EV239

(Steenbergen et al. 1992) was used to inoculate a 5 mL LB medium culture supplemented with 40 μg/mL ($^{13}C_U$, ^{15}N) *N*-acetylneuraminic acid, 50 μg/mL kanamycin and 12.5 μg/mL tetracycline for ~20 h. The medium was then replaced by washing cells, pelleted in an IEC clinical centrifuge, 2 times with 5 mL 1-times phosphate buffered saline, and finally gently resuspended in 300 μL of fresh wash solution (supplemented with 10% D_2O). This mixture was transferred to a 4 mm NMR tube for observation. Isotope-enriched (99% ^{13}C) monomeric and polymeric *N*-acetylneuraminic acid was prepared as described (Azurmendi et al. 2007). For the NMR sample, 2.4 mg of polymeric *N*-acetylneuraminic acid was dissolved in ~300 μL D_2O and placed in a 4 mm NMR tube.

Preparation of $^{13}C_{1,2,3}$-*N*-acetylneruaminic acid-labeled immunoglobulin G Fc

Isotope-enriched (>95%) *N*-acetylneuraminic acid ($^{13}C_{1,2,3}$) was prepared according to published reports (Aubin and Prestegard 1993; Simon et al. 1988). Human IgG Fc (10 mg, Athens Research and Technology, Athens GA) was desialylated and galactosylated, then sialylated with $^{13}C_{1,2,3}$-*N*-acetylneuraminic acid using published procedures to produce a uniformly galactosylated glycan with a sialic acid (>95%) on the α1-3 branch of the Asn297 *N*-glycan (Barb et al. 2009). IgG Fc was purified using a Protein A Sepharose column (GE Healthcare) and placed in a buffer containing 25 mM sodium phosphate, 100 mM potassium chloride and 1 mM DSS, pH 7.0 in 100% D_2O. The final NMR sample contained ~0.5 mM $^{13}C_{1,2,3}$-*N*-acetylneuraminic acid-terminated glycan.

NMR spectroscopy

NMR experiments were collected on a 21.1 T spectrometer equipped with a Varian VNMRS console and a 5 mm cryogenically-cooled probe. The samples were observed at 25°C with the exception of IgG Fc, which was observed at 25 or 50°C. NMR experiments were conducted using the Varian VNMRJ software (ver 2.3A) with the BioPack upgrade. NMR data were processed using NMRPipe (Delaglio et al. 1995) and analyzed using NMRViewJ (One Moon Scientific, Westfield, NJ).

Results

H3–C2 correlation

A fundamental challenge in detecting ^{13}C-labeled molecules in complex mixtures (in or on living tissue, for example) is suppressing undesirable background signals which may be 100s–1,000s of fold more intense. In traditional NMR acquisitions (a ^1H–^{13}C HSQC experiment, for example) these signals arise from the ~1% natural abundance of ^{13}C in cellular metabolites. The unwanted signals are reduced 90-fold to 100-fold when compared to detected signals from a 90–100% enriched ^{13}C-labeled molecule at equal concentrations, but this reduction often cannot be achieved when lipids and certain metabolites with considerable spectral overlap exist at 10 s of mM concentrations. Additional suppression of background signals (up to 100-fold) could be achieved, in principle, by detecting ^{13}C–^{13}C pairs in the molecules of interest. Further enhancements may be achieved by applying band-selective radio-frequency (rf) pulses and pulsed field gradients to select coherences of interest.

The first NMR experiment presented was designed to detect sialic acid residues on living cells with high sensitivity and exceptional background suppression capabilities. The pulse strategy is shown in Fig. 2a. It transfers magnetization from the H3 protons, through C3 to C2 via a small number of band-selective ^{13}C pulses which refocus or invert magnetization. The magnetization evolution pathway to the point following the pulse marked $\phi 2$ is

$$H3_z \rightarrow -H3_z\,C3_z \rightarrow 2H3_z\,C3_x\,C2_z \rightarrow -2H3_z\,C3_z\,C2_x$$

This operator is allowed to evolve under the chemical shift of the C2 carbon while the effect of scalar C3 and C1 coupling is removed with an amplitude-modulated band-selective pulse. Next, the τ_f/p.f.g.(4) → refocus → τ_f/p.f.g.(4) element eliminates single ^1H–^{13}C coherences that have leaked through the sequence. This provides an additional filtering mechanism. The coherence is then converted to pure $H3_x$ for detection.

The benefit of the aggressive background suppression in detecting the H3–C2 sialic acid correlations on living *E. coli* EV239 cells is illustrated in Fig. 3. EV239 cells are a K12 strain engineered to contain a K1-type capsule [poly-*N*-acetylneuraminic acid (pSA)] (Steenbergen et al. 1992; Vimr 1992). The traditional ^1H–^{13}C HSQC experiment shows correlations between other ^1H–^{13}C pairs, including the *N*-acetylneuraminic acid *N*-acetyl and some unidentified background metabolite peaks (Fig. 3a). These unwanted signals are absent in Fig. 3b owing to the efficient removal by the numerous filter elements. Initial attempts to collect the H3–C2 coherence suffered from substantial t_1 noise in samples containing high background metabolite signals (data not shown). This noise was largely eliminated by the addition of the C2 refocusing element after C2 chemical shift evolution (described above).

The benefit of separating sialic acid signals based on the C2 chemical shift is shown in Fig. 3b. Three forms of the *N*-acetylneuraminic acid are seen: the monomeric form which exists primarily as the β anomer, a polymeric α2-8-

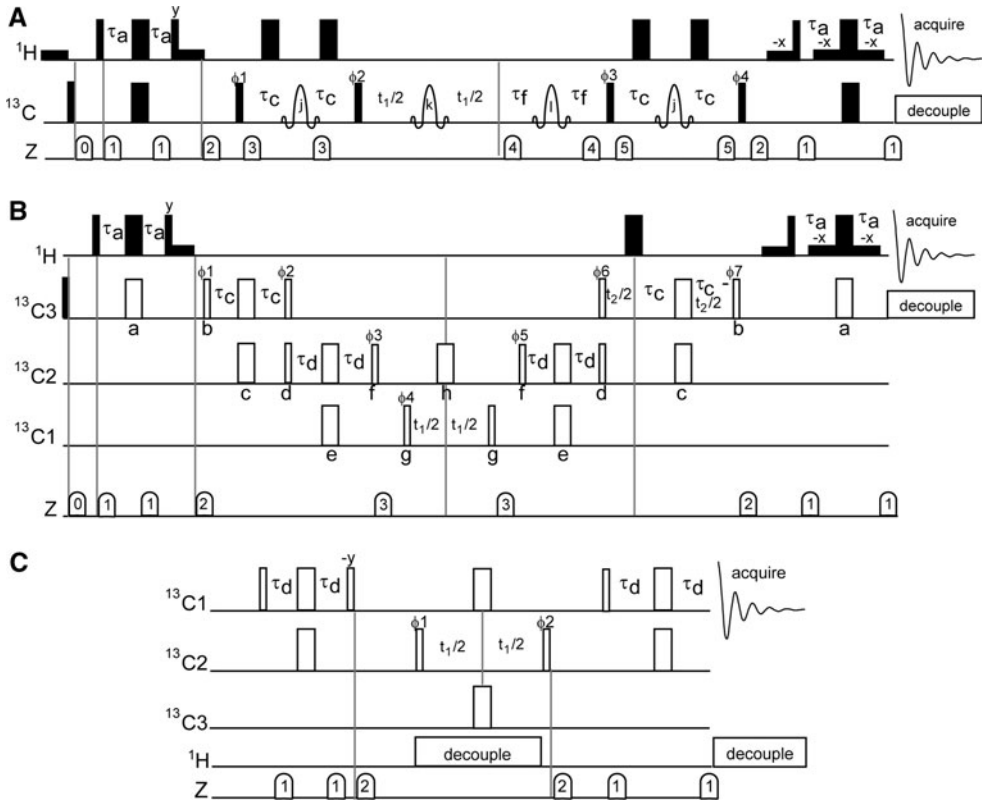

Fig. 2 Pulse sequences specific for sialic acids utilize single quantum coherences. **a** An experiment that correlates the H3 nuclei with C2 utilizes band-selective carbon refocusing and inversion pulses to prepare the desired coherences effectively filters unwanted signals. *Narrow* (wide) *rectangles* indicate 90° (180°) pulses. The pulse marked "*j*" is a polychromatic selective REBURP (Geen and Freeman 1991) pulse with 20 ppm bandwidth centered at two frequencies (102 ppm and 43 ppm). "*k*" is a square 180° pulse to decouple C1 and C3 during C2 chemical shift evolution, is centered at 175 and 43 ppm, and is only applied when t1 is greater than the time required to apply this pulse. "*l*" is a 20 ppm C2-selective REBURP pulse centered at 102 ppm. The transfer delay τ_a is 1/4JCH (1.85 ms), τ_c is 1/4JC3-C2 (5.8 ms), τ_f is 650 μs. The gradient delays (ms), and levels (G/cm) are: **0**: 1.0, 9; **1**: 0.3, 18; **2**: 1.0, 21; **3**: 0.6, 15; **4**: 0.5, −14; **5**: 0.5, 1. The phase cycling is $\phi1 = \{x, -x\}$; $\phi2 = \{2(y), 2(-y)\}$; $\phi3 = \{4(y), 4(-y)\}$; $\phi4 = \{8(x), 8(-x)\}$; $\phi rec = \{4(x, -x), 4(-x, x)\}$. Quadrature detection is achieved according to the STATES-TPPI method (Marion et al. 1989) by modulating the coherence orientation in a stepwise fashion: 1 ($\phi1$, $\phi2$ and ϕrec as stated), 2($\phi1$ and $\phi2 + 90°$, ϕrec as stated), 3 ($\phi1$, $\phi2$ and ϕ rec + 180°, ϕrec as stated) and 4 ($\phi1$ and $\phi2 + 270°$, $\phi rec + 180°$). *Horizontal black rectangles* represent water flip-back pulses (∼1.2 ms *rectangular pulses*). **b** An experiment that correlates the H3 nuclei with C1 utilizes band selecting excitation, refocusing and inversion pulses. The first pulse (marked with a *) is the only broad-band carbon pulse. All remaining carbon pulses, shown as *hollow narrow* (wide) *rectangles* are band-selective 90° (180°) pulses centered at the nucleus indicated (C3: 43 ppm, C2: 102 ppm, C1: 175 ppm). The pulse characteristics are given in Table 1. The transfer delay τ_d is 1/4JC2–C1 (4.0 ms). The gradient delays (ms) and levels (G/cm) are: **0**: 1.0, 9; **1**: 0.3, 5; **2**: 1.0, 21; **3**: 1.4, 21. The phase cycling is $\phi1 = \{x, -x\}$; $\phi2 = \{2(y), 2(-y)\}$; $\phi3 = \{-x\}$; $\phi4 = \{4(x), 4(-x)\}$; $\phi5 = \{8(y), 8(-y)\}$; $\phi6 = \{4(x), 4(-x)\}$; $\phi7 = \{y\}$; $\phi rec = \{x, -x, -x, x, 2(-x, x, x, -x), x, -x, -x, x\}$. Quadrature detection is achieved according to the STATES-TPPI method by modulating $\phi4$ and ϕrec. This sequence is also capable of collecting the C2 chemical shift in a three dimensional experiment. Quadrature in this circumstance is achieved by STATES-TPPI modulation of $\phi7$ and ϕrec. **c** A C1–C2 experiment collects C1 and C2 chemical shifts as well as the one-bond C1–C2 scalar coupling at high resolution. Each pulse in this sequence is band-selective at the nucleus indicated with *narrow* (wide) *rectangles* indicating 90° (180°) pulses. Refocusing and inversion during the INEPT (Morris and Freeman 1979) periods is achieved using polychromatic selective REBURP pulses centered at 176 and 102 ppm with 25 ppm bandwidths. 90° pulses are executed using the EBURP1 (Geen and Freeman 1991) shape with a 25 ppm bandwidth at the indicated frequency. The central 180° pulse decouples C1 and C3 from C2 evolution using a polychromatic Gauss 180 pulse with 20 ppm bandwidths. Proton decoupling is achieved with continuous wave decoupling during both periods. The gradient delays (ms) and levels (G/cm) are: **1**: 0.5, 9; **2**: 1.0, 21. The phase cycling is $\phi1 = \{2(x), 2(-x)\}$; $\phi2 = \{-x, x\}$; $\phi rec = \{x, -x, -x, x\}$. Quadrature detection is achieved according to the STATES-TPPI method by modulating $\phi1$ and ϕrec

linked pSA, and a form consistent with a polymeric α2-8 linkage that has undergone a condensation (between the C1 carboxylate and the C8 hydroxyl of the preceding residue) to form a lactone (pSA-lactone, Azurmendi et al. 2007). The C3 chemical shifts of these species are similar, but there is a large difference between the pSA and pSA-lactone C2 chemical shifts. In addition, resolving species with the C2 shift offers the potential for higher resolution

Table 1 Pulse parameters for the H3–C1 correlation experiment

Pulse	Function	Shape	Bandwidth (ppm)
a	Invert C3	REBURP[a]	20
b	90° C3	Half gaussian	20
c	Refocus C3, invert C2	REBURP, REBURP[a]	15, 15
d	Return C3 to Z, 90° C2	Half gaussian, half gaussian	15, 15
e	Refocus C2, invert C1	REBURP, REBURP[a]	15, 15
f	Return C2 to Z	Square 90°	25
g	90° C1	Square 90°	25
h	Invert C2	Square 180°	30

[a] Geen and Freeman (1991)

spectra in the indirect dimension when using complex samples because the C2 linewidths at 21.1T are considerably less than the C3 linewidths (data not shown). An added benefit of increased resolution with the C2 chemical shift is the ability to separate signals with a reduced acquisition time in the indirect dimension when compared to C3. This is advantageous when observing peaks with increased R_2 relaxation rates, as would be expected for large glycoproteins or cell-surface glycans.

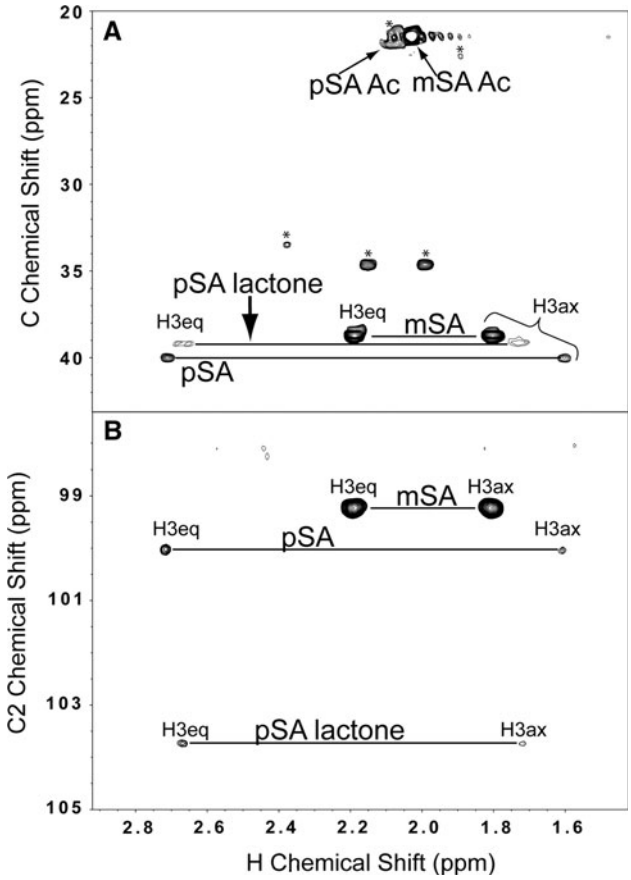

Fig. 3 Application of the H3–C2 correlation experiment to the capsular pSA polysaccharide on *E. coli* EV239 cells demonstrates the selectivity and sensitivity of the method. **a** A ^{13}C HSQC spectrum reveals the H3–C3 *N*-acetylneuraminic acid coherences as well other H–^{13}C pairs from intact *E. coli* cells. This experiment was collected using 16 scans/increment, 128 increments and a ^{13}C sweep width of 20 kHz. **b** The three forms of the *N*-acetylneuraminic acid are clearly resolved and background signals are effectively removed using the H3–C2 correlation experiment which collects the resonance frequencies of the H3 and C2 nuclei. This experiment was collected using 128 scans/increment, 96 increments and a ^{13}C sweep width of 3.6 kHz

H3–C1 correlation

The C1 chemical shift may also be used as a probe for glycan structure and dynamics and is more sensitive to the ionization state of the carboxylate group than C2. Thus, we devised a method which utilizes a similar background filtering and coherence transfer principle as the H3–C2 experiment to correlate signals from the H3 and C1 nuclei of sialic acid (Fig. 2b). This approach utilizes a greater number of band-selective excitation, refocusing and inversion pulses to separately perturb the C1, C2 and C3 nuclei, which, in principle, should possess even greater background suppression qualities. The coherence preparation proceeds in a similar manner to that of the H3–C2 experiment, except the temporally separated band-selective 90° ^{13}C pulses permit insertion of crush gradients while the magnetization is parallel to the z axis.

Following the pulse marked $\phi 3$, the coherence pathway is as follows:

$$\begin{aligned} &8H3_z\,C3_z\,C2_z\,C1_z \rightarrow -8H3_z\,C3_z\,C2_z\,C1_x \\ &\rightarrow t_1 \rightarrow -8H3_z\,C3_z\,C2_z\,C1_z \rightarrow -8H3_z\,C3_z\,C2_x\,C1_z \rightarrow \\ &\quad -4H3_z\,C3_z\,C2_y \rightarrow 4H3_z\,C3_y\,C2_z \\ &\rightarrow -2H3_z\,C3_x \rightarrow 2H3_y\,C3_z \rightarrow H3_x \rightarrow \text{detect} \end{aligned}$$

The effect of C2–C1 scalar coupling is removed with a band-selective C2 inversion pulse if the t_1 increment is greater than the time necessary to apply this pulse.

An H3–C1 correlation spectrum of the 55 kDa mono-$^{13}C_{1,2,3}$-sialylated IgG Fc molecule (one sialic acid per glycan) is shown and compared to H3–C3 and H3–C2 correlation spectra in Fig. 4. The Fc domain of Immunoglobulin G is a dimer with two complex-type, biantennary glycans. The structure of these glycans is related to

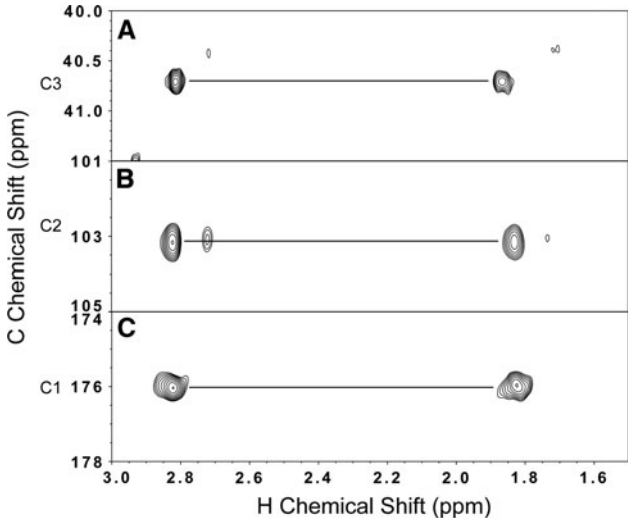

Fig. 4 The application of these methods reveals the H3, C3, C2 and C1 chemical shifts of the 55 kDa ^{13}C-monosialylated IgG1 Fc. **a** A ^{13}C HSQC spectrum with C2 refocusing applied during C3 chemical shift evolution. This experiment was collected using 160 scans/increment, 128 increments and a ^{13}C sweep width of 1 kHz. The H3–C2 (**b**) and H3–C1 (**c**) correlation experiments reveal the chemical shifts of the non-protonated C2 and C1. The weaker set of peaks seen in **a** and **b** likely result from degraded Fc. The H3–C2 experiment was collected using 512 scans/increment, 32 increments and a ^{13}C sweep width of 10 kHz. The H3–C1 experiment was collected using 1,024 scans/increment, 26 increments and a ^{13}C sweep width of 6 kHz

autoimmune disease (Parekh et al. 1985) and these glycans have been shown to be mobile but constrained by the Fc polypeptide surface (Barb and Prestegard 2011). This sample contains a biantennary glycan with a single sialic acid residue at the α1-3 Man branch terminus of the glycan (Barb et al. 2009). The correlations for this sialic acid residue are clearly seen and occur at the expected carbon chemical shift values. The H3–C1 sequence has similar background filtering properties as the H3–C2 experiment, but suffers somewhat from reduced sensitivity when compared to the H3–C2 experiment, likely owing to the reduced efficacy resulting from the greater number of shaped pulses and the coherence attenuation by spin relaxation during the magnetization transfer periods. These correlations may be stronger at lower magnetic fields where the effect of carbonyl carbon CSA relaxation is smaller.

C1–C2 correlation

Alternative approaches must be employed when detecting sialic acids with unfavorable dynamic properties. As molecular mass increases, due to polymerization or coordination by a large molecule, rotational correlation times become long. At this limit, experiments utilizing proton resonances and heteronuclei with directly bonded protons suffer a disadvantage due to their short transverse relaxation times. Therefore, non-protonated carbon atoms become useful spectroscopic probes because they are less affected by decreased correlation times. Indeed, NMR experiments to assist in the assignment of backbone polypeptide resonances have been designed that bypass H nuclei entirely (Takeuchi et al. 2010a, b). These methods are additionally effective when characterizing nuclei in the presence of paramagnetic centers (Otting 2008), or nuclei that experience line-broadening by chemical exchange, as is the case for some of the sites on IgG Fc glycans. It is therefore of interest to develop an NMR experiment to observe sialic acid that utilizes only the non-protonated carbons in sialic acids.

A selective ^{13}C–^{13}C correlation experiment designed to measure the C1 and C2 chemical shifts is shown in Fig. 5. This experiment is analogous to a heteronuclear single quantum coherence pulse sequence except that a coherence is observed between different carbon frequencies is observed (Bodenhausen and Ruben 1980; Morris and Freeman 1979). Detecting the C1 nucleus directly is preferable to detecting C2 when using a $^{13}C_{1,2,3}$-labeled residue. The C1 signal at resolutions achievable with large molecules shows the effect of a single resolved homonuclear scalar coupling with C2, while the C2 signal appears as a quartet due to the presence of two unequal and resolved scalar couplings to C1 and C3 (62 and 43 Hz, respectively, for the α anomer). In this experiment, equilibrium $C1_z$ magnetization is transformed into the

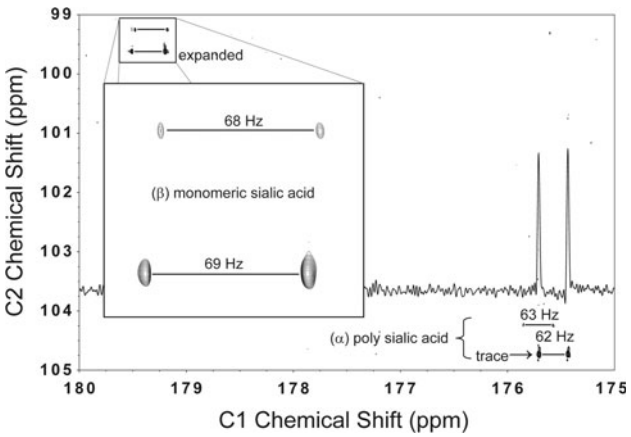

Fig. 5 A C1–C2 correlation spectrum of purified polysialic acid shows both monomeric sialic acid, mostly as a β anomer, and the polysialic acid which is α2-8 linked. The scalar C1–C2 couplings are reported for each of the doublets observed. The *inset* shows an enlargement of the β-sialic acid cross peaks. The one-dimensional spectrum is taken through the α-polysialic acid doublet. This experiment was collected using 4 scans/increment, 220 increments and a ^{13}C2 sweep width of 2.5 kHz. Complex points (4096) were collected with a spectral width of 22 kHz in the direct dimension and processed with a 1 Hz Gaussian multiplier window function

antiphase $C1_zC2_x$ operator and frequency labeled with the C2 chemical shift. During the chemical shift evolution the effects of C3 and C1 scalar couplings are removed by band-selective inversion of these resonances (when allowed by the length of the t_1 period). The $C1_zC2_z$ operator, created following a 90° C2 pulse, is transformed into magnetization proportional to $C1_yC2_z$ which is then refocused into pure in-phase $C1_x$ magnetization for detection. Proton decoupling during acquisition is included to remove the effect of the three bond H3(ax)–C1 scalar coupling which is $\sim$1.5 Hz for the α anomer.

This sequence has background suppression properties like the other two experiments. This is due to the exploitation of two sequential ^{13}C nuclei resulting in a 10,000-fold enhancement of labeled $^{13}C_{1,2,3}$-*N*-acetylneuraminic acid over unlabeled background molecules, in addition to suppressive properties of narrow bandwidth pulses. This experiment will not be as sensitive as the preceding sequences when detecting molecules with short correlation times as a result of the reduced levels of ^{13}C polarization (1/4th of ^{1}H) and the reduced sensitivity of ^{13}C detection (1/16th of ^{1}H) when compared to ^{1}H excite/detect experiments, however, for large molecules with long correlation times, losses during multiple coherence transfer and refocusing steps to and from protons, will more than cancel sensitivity gains.

A C1–C2 correlation spectrum collected using a sample containing a mixture of purified poly and monomeric sialic acid is shown in Fig. 5 and provides an indication of the linewidths that were achieved. This spectrum shows the resolution of the experiment achieved by exploiting both the C1 and C2 carbon chemical shift differences. The peaks of less intensity above both the dominant mono and polysialic acid crosspeaks likely reflect degradation in the sample.

This experiment also provides a direct measure of the 1-bond C1–C2 scalar coupling values with very high precision (Fig. 5). The H3(ax)–C1 coupling would be resolved in a higher resolution spectrum.

Discussion

Development of experiments designed for studies of carbohydrates have lagged behind experiments developed for the study of proteins and nucleic acids. It is appropriate to point out that the H3–C2 correlation pulse sequence was inspired by a set of experiments designed by Prof. Kay and Prof. Tugarinov for the assignment for Ile, Leu and Val methyl groups in proteins (Tugarinov and Kay 2003). These experiments were some of several that extended the capability of NMR spectroscopy to the study of large, highly deuterated proteins. The carbohydrate-specific NMR methods presented here in a small way expand the selection of experiments available to the glycobiology community.

These experiments are particularly applicable to a variety of sialic acid-containing biomolecules, including the purified polysaccharides (Fig. 5), glycoprotein glycans on large molecules (Fig. 4), and cell surface carbohydrates (Fig. 3) presented here. These methods are also applicable to many different types of sialic acids that share the same C1 carboxylate–C2 anomeric–C3 methylene carbon motif, including those residues shown in Fig. 1. These pulse sequences require no modification to function with both $^{13}C_U$- and $^{13}C_{1,2,3}$-enriched *N*-acetylneuraminic acid and effectively reduce the background signals of undesirable cellular metabolites.

One potential asset of the methods presented is the ability to resolve resonances from sialic acid residues in different environments, using multiple carbon chemical shifts. *N*-glycans, for example, can contain one, two, three or four antenna that can be modified with single terminal sialic acid residues in either an α2-3 or α2-6 linkage (Varki 2009). In addition, poly α2-8-linked sialic acid chains hundreds of residues long are also attached to some *N*-glycans (Nelson et al. 1995). *N*-glycosylation often occurs at multiple sites on a protein, and different glycans on the same protein are remodeled to different final structures with potentially distinct functions. The multiple sources of chemical diversity provide a great challenge for structural methods, but these sequences are a multi-dimensional tool to separate signals from individual units and ultimately study the mechanisms behind glycan function.

The H3–C2 correlation experiment proved to be the most sensitive of the three using the conditions presented here. With stable samples such as glycoproteins the detection limit for these experiments is much lower than the spectra presented, given that ample experimental time is available. Using cell cultures, however, the detection limit is likely restrained by the amount of labeled material metabolized by the cell and experimental collection time is limited by the length of time the culture can withstand the environment in the NMR tube (likely no more than 24 h). The H3–C2 spectrum in Fig. 3 using *E. coli* EV239 cells was collected for 9.5 h.

These methods are also suited for measuring structural restraints in the form of residual dipolar couplings (RDCs). RDCs provide information on how chemical bond vectors, and molecules to which they are attached, orient in a partially aligning medium. These too are capable of providing high resolution information on glycan orientation and structure (Prestegard et al. 2004). With the $^{13}C_{1,2,3}$-*N*-acetylneuraminic acid labeling, couplings from multiple, non-colinear bonds provide highly complementary information as to the orientation of the carbohydrate residue. By removing decoupling pulses from these experiments, it is

possible to measure with high precision RDCs from four dipole pairs, including C1–C2, C2–C3, H3(ax/eq)–C3, and C1–H3ax. The most sensitive experiment, the H3–C2 correlation, is capable of providing data to measure the first three of these values. In combination with other new methods (Liu and Prestegard 2010), residual chemical shift anisotropy values which, similar to RDCs are indicative of orientation, may also be measured with high precision.

These pulse sequences may also be used to measure distance and orientation information in relation to a paramagnetic center. Defining conformation about the glycosidic residue–residue linkage is challenging due the few protons nearby. Paramagnetic centers offer a complementary approach via paramagnetic relaxation enhancement and pseudocontact shifts. These can be measured by simply observing chemical shifts and intensities (Otting 2008). The C1–C2 experiment in particular offers an advantage in allowing observation at distances where broadening of protons lines prevents use of proton detected experiments.

Acknowledgments We thank Dr. Eric Vimr (U. Illinois) for the *E. coli* EV239 cells, and Dr. Yizhou Liu and Dr. Xu Wang for helpful discussions regarding pulse sequence design. This work was financially supported by the grants RO1GM033225 and P41RR005351 from the National Institutes of Health. A.W.B. was supported by a NIH Kirschstein National Research Service Award (F32AR058084). The content of this work is solely the responsibility of the authors and does not necessarily represent the official views of the NIH.

References

Aubin Y, Prestegard JH (1993) Structure and dynamics of sialic-acid at the surface of a magnetically oriented membrane system. Biochemistry 32:3422–3428

Azurmendi HF, Vionnet J, Wrightson L, Trinh LB, Shiloach J, Freedberg DI (2007) Extracellular structure of polysialic acid explored by on cell solution NMR. Proc Natl Acad Sci USA 104:11557–11561

Barb AW, Prestegard JH (2011) NMR analysis demonstrates immunoglobulin G *N*-glycans are accessible and dynamic. Nat Chem Biol 7:147–153

Barb AW, Brady EK, Prestegard JH (2009) Branch-specific sialylation of IgG-Fc glycans by ST6Gal-I. Biochemistry 48:9705–9707

Bhattacharjee AK, Jennings HJ, Kenny CP, Martin A, Smith IC (1975) Structural determination of the sialic acid polysaccharide antigens of neisseria meningitidis serogroups B and C with carbon 13 nuclear magnetic resonance. J Biol Chem 250: 1926–1932

Bodenhausen G, Ruben DJ (1980) Natural abundance N-15 Nmr by enhanced heteronuclear spectroscopy. Chem Phys Lett 69: 185–189

Brockhausen I (2006) Mucin-type O-glycans in human colon and breast cancer: glycodynamics and functions. EMBO Rep 7: 599–604

Delaglio F, Grzesiek S, Vuister GW, Zhu G, Pfeifer J, Bax A (1995) Nmrpipe—a multidimensional spectral processing system based on UNIX pipes. J Biomol NMR 6:277–293

Geen H, Freeman R (1991) Band-selective radiofrequency pulses. J Magn Reson 93:93–141

Gerken TA, Dearborn DG (1984) Carbon-13 NMR studies of native and modified ovine submaxillary mucin. Biochemistry 23:1485–1497

Liu Y, Prestegard JH (2010) A device for the measurement of residual chemical shift anisotropy and residual dipolar coupling in soluble and membrane-associated proteins. J Biomol NMR 47:249–258

Marion D, Ikura M, Tschudin R, Bax A (1989) Rapid recording of 2d Nmr-spectra without phase cycling—Application to the study of Hydrogen-Exchange in Proteins. J Magn Reson 85:393–399

Melrose J, Fuller ES, Roughley PJ, Smith MM, Kerr B, Hughes CE, Caterson B, Little CB (2008) Fragmentation of decorin, biglycan, lumican and keratocan is elevated in degenerate human meniscus, knee and hip articular cartilages compared with age-matched macroscopically normal and control tissues. Arthritis Res Ther 10:R79

Morris GA, Freeman R (1979) Enhancement of nuclear magnetic-resonance signals by polarization transfer. J Am Chem Soc 101: 760–762

Muramatsu T, Muramatsu H (2004) Carbohydrate antigens expressed on stem cells and early embryonic cells. Glycoconj J 21:41–45

Nacher J, Guirado R, Varea E, Alonso-Llosa G, Rockle I, Hildebrandt H (2010) Divergent impact of the polysialyltransferases ST8Sia-II and ST8SiaIV on polysialic acid expression in immature neurons and interneurons of the adult cerebral cortex. Neuroscience 167:825–837

Nasirikenari M, Segal BH, Ostberg JR, Urbasic A, Lau JT (2006) Altered granulopoietic profile and exaggerated acute neutrophilic inflammation in mice with targeted deficiency in the sialyltransferase ST6Gal I. Blood 108:3397–3405

Nelson RW, Bates PA, Rutishauser U (1995) Protein determinants for specific polysialylation of the neural cell adhesion molecule. J Biol Chem 270:17171–17179

Otting G (2008) Prospects for lanthanides in structural biology by NMR. J Biomol NMR 42:1–9

Parekh RB, Dwek RA, Sutton BJ, Fernandes DL, Leung A, Stanworth D, Rademacher TW, Mizuochi T, Taniguchi T, Matsuta K et al (1985) Association of rheumatoid arthritis and primary osteoarthritis with changes in the glycosylation pattern of total serum IgG. Nature 316:452–457

Prestegard JH, Bougault CM, Kishore AI (2004) Residual dipolar couplings in structure determination of biomolecules. Chem Rev 104:3519–3540

Reis CA, Osorio H, Silva L, Gomes C, David L (2010) Alterations in glycosylation as biomarkers for cancer detection. J Clin Pathol 63:322–329

Simon ES, Bednarski MD, Whitesides GM (1988) Synthesis of Cmp-Neuac from N-Acetylglucosamine—generation of Ctp from Cmp using adenylate kinase. J Am Chem Soc 110:7159–7163

Skehel JJ, Wiley DC (2000) Receptor binding and membrane fusion in virus entry: the influenza hemagglutinin. Annu Rev Biochem 69:531–569

Steenbergen SM, Wrona TJ, Vimr ER (1992) Functional analysis of the sialyltransferase complexes in *Escherichia coli* K1 and K92. J Bacteriol 174:1099–1108

Takeuchi K, Frueh DP, Hyberts SG, Sun ZY, Wagner G (2010a) High-resolution 3D CANCA NMR experiments for complete mainchain assignments using C(alpha) direct detection. J Am Chem Soc 132:2945–2951

Takeuchi K, Heffron G, Sun ZY, Frueh DP, Wagner G (2010b) Nitrogen-detected CAN and CON experiments as alternative experiments for main chain NMR resonance assignments. J Biomol NMR 47:271–282

Theocharis AD, Skandalis SS, Tzanakakis GN, and Karamanos NK (2010) Proteoglycans in health and disease: novel roles for proteoglycans in malignancy and their pharmacological targeting. FEBS J 277:3904–3923

Tugarinov V, Kay LE (2003) Ile, Leu, and Val methyl assignments of the 723-residue malate synthase G using a new labeling strategy and novel NMR methods. J Am Chem Soc 125:13868–13878

Varki A (2007) Glycan-based interactions involving vertebrate sialic-acid-recognizing proteins. Nature 446:1023–1029

Varki A (2009) Essentials of glycobiology. Cold Spring Harbor Laboratory Press, Cold Spring Harbor

Vimr ER (1992) Selective synthesis and labeling of the polysialic acid capsule in *Escherichia coli* K1 strains with mutations in nanA and neuB. J Bacteriol 174:6191–6197

Witsch-Prehm P, Miehlke R, Kresse H (1992) Presence of small proteoglycan fragments in normal and arthritic human cartilage. Arthritis Rheum 35:1042–1052